



## Effect of radial hydride on delayed hydride cracking behaviour of Zr-2.5Nb pressure tube material

Saurav Sunil<sup>a</sup>, Avinash Gopalan<sup>a</sup>, A.K. Bind<sup>a</sup>, R.K. Sharma<sup>b</sup>, T.N. Murty<sup>a</sup>, R.N. Singh<sup>a,\*</sup>

<sup>a</sup> Mechanical Metallurgy Division, Bhabha Atomic Research Centre, Trombay, Mumbai 400085 India

<sup>b</sup> Engineering Directorate, Nuclear Power Corporation of India Limited, Anushaktinagar, Mumbai 400094, India



### ARTICLE INFO

#### Article history:

Received 5 May 2020

Revised 9 August 2020

Accepted 10 August 2020

Available online 14 August 2020

#### Keywords:

Zr-2.5Nb PT material

Delayed hydride cracking

Radial hydride

Hydride continuity coefficient

### ABSTRACT

Delayed Hydride Cracking (DHC) behaviour of Zr-2.5Nb Pressure Tube (PT) material used in Indian 200MWe Pressurised Heavy Water Reactor (PHWR) containing radial hydrides and circumferential hydrides was studied in the temperature range of 200–250 °C. A section of the PT was charged with 70wppm of hydrogen and successfully subjected to re-orientation treatment to form radial hydride. The radial hydride in the reoriented tube was characterised by the hydrogen continuity co-efficient (HCC). It was observed that the average DHC velocity ( $V_{DHC}$ ) for the radial hydrided sample was 2.5 and 1.85 times faster than the circumferential hydrided sample at 200 and 225 °C, respectively. The  $V_{DHC}$  at the temperature of 250 °C, for both the radial hydrided and the circumferential hydrided sample were comparable. The average  $V_{DHC}$  for circumferential hydrided sample varies linearly with  $1/T$  while it was observed to vary non-linearly with  $1/T$  for radial hydrided sample. The  $V_{DHC}$  of the radial hydrided sample was observed to increase with increase in the stress intensity factor, whereas for circumferential hydrided samples the  $V_{DHC}$  was independent of stress intensity factor in the range of 18–45MPa.m<sup>1/2</sup>.

© 2020 Elsevier B.V. All rights reserved.

### 1. Introduction

Zr-2.5Nb Pressure Tube (PT) is a pressure boundary component used in the Pressurised Heavy Water Reactor (PHWR) [1–4]. During the service of the PHWR, PTs pick up hydrogen isotopes primarily due to the corrosion reaction [5]. The hydrogen isotopes concentration increases with the operating duration of the reactor. On exceeding the terminal solid solubility in Zr alloys, hydrogen precipitate as brittle phases in the form of hydrides of plate shaped morphology. These hydrides affect the structural integrity of the PT material due to reduction in fracture toughness, crack growth by delayed hydride cracking (DHC) and enhanced hydride blister formation susceptibility.

The crystallographic texture of the Zr-2.5Nb PT material is such that abundantly two orientations of the hydride are present [4, 6]. These are along the circumferential-axial plane and along the radial-axial plane [7]. Hydride platelets oriented along the circumferential-axial plane are called the circumferential hydrides and those oriented along the radial-axial plane are called the radial hydrides. The circumferential hydrides form in Zr-2.5Nb PT under normal reactor operating conditions. To form the radial hydrides a

threshold stress for reorientation is required for the hydride reorientation. The radial hydride formation in the PT during the reactor operation is avoided by keeping the stresses below the threshold stress for reorientation. However, in the presence of residual tensile stress especially in the regions near to the rolled joint [7–10] and due to in-service wall thickness reduction, the net stress may exceed the threshold stresses to form the radial hydrides.

The presence of the radial hydride in PT reportedly reduces the ductility and fracture toughness drastically as compared to the PT containing circumferential hydride at room temperature [6, 11–13]. The brittle to ductile transition temperature for the PT containing radial hydride is also higher as compared to the PT containing circumferential hydride [12, 13]. The influence of the radial hydride on the fracture toughness of the PT has been characterized as a function of the hydride orientation (termed as hydride continuity coefficient (HCC)) with temperature [11]. The operator response time is an important parameter for the safe operation of reactor. It determines the time required for the operator to respond to an incident. To calculate the operator response time, critical crack length (CCL) and DHC Velocity ( $V_{DHC}$ ) are required.

In the literature, DHC phenomenon of the Zr-2.5Nb PT is well documented [14–22]. DHC is usually associated with an incubation period to crack initiation, a stable average crack growth velocity called the DHC velocity ( $V_{DHC}$ ) and a threshold stress intensity factor ( $K_{IH}$ ). The  $V_{DHC}$  is influenced to a varying degree by the test

\* Corresponding author.

E-mail address: [rnsingh@barc.gov.in](mailto:rnsingh@barc.gov.in) (R.N. Singh).

**Table 1**

Tensile properties of Zr-2.5Nb PT material in transverse direction of the PT [30].

Material Temperature, °C	Conventional YS, MPa	Indian CWSR UTS, MPa
25	688	809
200	550	605
225	525	583
250	500	560

**Table 2**

Elastic and Plastic properties of Zr-2.5Nb PT material at 200 °C.

Flow stress	Plastic strain
556.1869	0.00E+00
560.3322	2.28E-03
574.8759	3.25E-03
599.2729	6.17E-03
615.3963	0.0108
620.9164	0.0157

temperature [14, 15, 17, 20], direction of approach of the test temperature [22], strength of the alloy [15, 17], hydrogen content [14, 15, 20], crystallographic texture and microstructure [18, 19, 21] of the material. However, till date data reported in the literature has been generated using samples that had either the hydrogen completely present in the solution or as circumferential hydride in the bulk during the DHC tests for Zr-2.5Nb PT material [14, 23–26]. Only a few studies are reported in the literature for the effect of radial hydride on the  $V_{DHC}$  of Zircaloy-4 cladding material [27]. Coleman et al. [28] reported that for DHC to occur, reoriented (radial) hydride is not required and the susceptibility to DHC depends on the extent of reorientation of the precipitated hydride. However, no study has been reported in the open literature on the effect of prior existing radial hydrides on the DHC behaviour of the Zr-2.5Nb PT material. The study of the DHC behaviour of Zr-2.5Nb PT material containing radial hydride in the bulk is required for safety assessment of this component under off-normal conditions.

The maximum permitted initial hydrogen concentration for quadruple melted Zr-2.5Nb PT material is 5wppm and the pickup rate is reported to be ~1wppm/yr in main body and ~2wppm/yr in rolled joint areas of the PT [29]. Considering the design life of the reactor to be 30 years, the end of life hydrogen concentration comes to be maximum approx. 35 and 65wppm in the main body and in the rolled joint areas of the PT, respectively. Hence Zr-2.5Nb PT material containing 70wppm of hydrogen concentration is used in the present investigation.

Thus, the objective of this work is to investigate the effect of prior existing radial hydrides on the  $V_{DHC}$  in the temperature range of 200–250 °C for Zr-2.5Nb PT material containing 70 wppm of hydrogen and to compare it with that of the material containing circumferential hydride and to rationalize the behaviour in terms of the HCC at the DHC test temperatures and hydride fracture zone volume.

## 2. Materials and experimental work

### 2.1. Material details and hydrogen charging

The Zr-2.5Nb PT manufactured by the conventional route was used in this study [25, 30]. The PT's were cold worked and stress relieved (CWSR), and manufactured from the quadruple melted ingots. The yield strength and tensile strength in transverse direction of the PT at 200, 225 and 250 °C were determined by miniature sample and is provided in Table 1. The details of the miniature sample are provided elsewhere [31]. A spool of 450mm was cut from the full-length PT and polished to remove the autoclaved layer from the inner and outer surfaces of the mid-section of the spool. The PT spool was charged with target hydrogen concentration of 70 wppm using the modified Sievert's apparatus [32]. The hydrogen concentration in the PT spool was subsequently determined using the Inert gas fusion technique (IGF) and was found to be in the 70±5wppm.

### 2.2. Re-orientation setup

The hydrogen charged spool was mounted in an internal pressurization setup as shown in the Fig. 1, where a hot fluid medium was used to pressurize the spool. During the pressurization it was insured that the hoop stress in the spool was greater than the re-orientation stress. The spool was heated to 350 °C to ensure all hydride dissolves back and tube was cooled to 300 °C then the pressure was increased to 20 MPa (hoop stress ~260 MPa) by pressurizing the fluid inside the spool to get the required stress for reorientation. The pressurized spool was thermally cycled under pressure between 300 °C and 200 °C to re-orient all the hydride to radial orientation and then finally cooled to room temperature under pressure. The schematic of the reorientation treatment process is shown in Fig. 2. Three thermocouples each at both the ends and one at the middle of the spool were mounted to monitor the temperature along the spool axis. The temperature variation was within ±4 °C.

### 2.3. Metallography and radial hydride characterisation

To study the DHC behaviour, 17 mm width curved CT (CCT) samples were machined from the spool subjected to reorientation treatment as well as from the as charged spool having circumferential hydrides. The CCT samples were made such that the crack direction was along the axial direction of the PT. The CCT samples were polished on the CR plane to obtain the micrographs. The CCT samples were polished up to 1200 grit paper and were etched with the 10:45:45 by volume (HF: HNO<sub>3</sub>: H<sub>2</sub>O) etchant to obtain the hydride micrographs. The HCC was evaluated for all the CCT samples cut from the radial hydride orientated spool. The HCC calculation is illustrated in the Fig. 3 [11, 13, 33]. For HCC calculation a box of 110 μm width is considered as shown in Fig. 3. Then assuming a light to be illuminated from one end of the box in the circumferential direction, the hydrides will cast a shadow on the other end of the box. The HCC is the ratio of the sum of the length of the shadows to the length of the box provided that the shadows are not less than 50 μm in length individually.

### 2.4. Finite element computation

The CT sample of the Zr-2.5Nb PT material was modelled as an elastic plastic isotropic material with properties mentioned in the Table 2. The flow stress at 200 °C was used for computation is also provided in the Table 2 as a function of plastic strain. The CT sample was considered as a 3D object symmetric about the  $y = 0$  plane and having width of 17mm from the load line, height of 10.2mm from the symmetry plane and a thickness of 4mm. The sample was meshed with 34,040 number of C3D8R elements totalling 38,621 nodes. Smaller elements were considered near the crack tip. The stress field around the crack tip was computed using commercial FEM package for a load of 2000N applied along the load line in 40 equal increments to obtain stress field as a function of stress

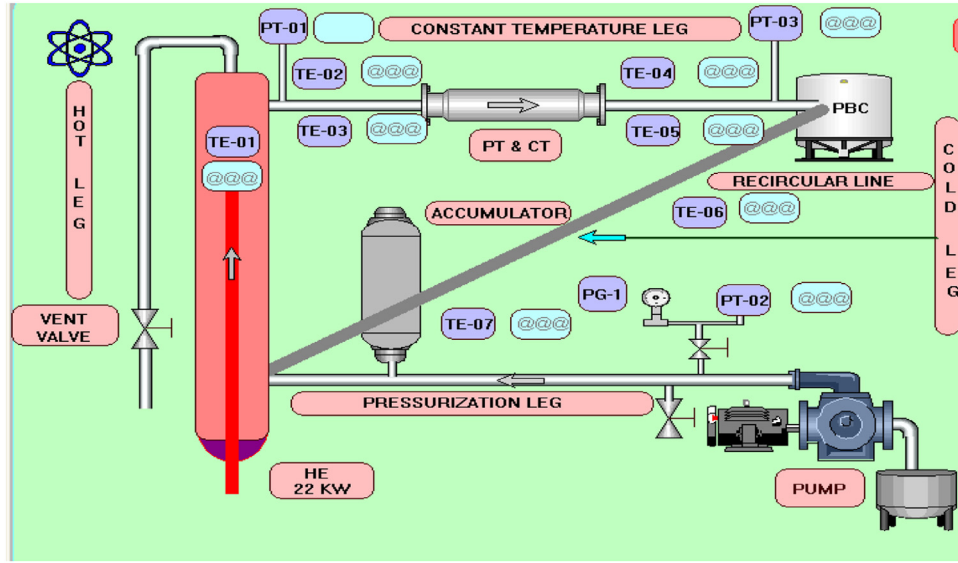


**Fig. 1.** Schematic of the radial hydride formation test setup.

intensity factor ( $K_I$ ). Using the principle stresses in  $y$  direction, hydride fracture zone was evaluated. Hydride fracture zone is defined by the region near to the crack tip where the principal stress perpendicular to the hydride platelet ( $\sigma_{yy}$  in present case) is sufficient to fracture the hydride platelet. The fracture criterion of the constrained hydride given by Shi and Puls [34] and represented by Eq. (1) was used.

$$\sigma_{yy} + \sigma^h \geq \sigma_f \quad (1)$$

where  $\sigma_{yy}$  is the principal stress perpendicular to hydride platelet,  $\sigma^h$  is the compressive stress due to hydride precipitation and  $\sigma_f$  is the fracture stress for the constrained hydride.

The criterion mentioned above is used to calculate the hydride fracture zone. The  $\sigma^h$  was taken to be 500 MPa [35] for the fully constrained long hydride and the fracture stress ( $\sigma_f$ ) of the hydride was taken to be 600 MPa [34, 36].

## 2.5. Pre-cracking and DHC testing

The HCC characterised CCT samples were pre-cracked in Rulmuc make resonant fatigue machine. Final stress intensity factor at the end of pre-cracking was about  $8\text{MPa}\sqrt{\text{m}}$ . The pre-cracking was carried out to extend the crack length to around 0.5 times ( $a/W$ ). The pre-cracked samples were then tested in the Zwick-Roell screw driven UTM fitted with the resistance heating three zone furnace to perform DHC tests. The test protocol used for the DHC testing are provided elsewhere [24]. The DHC test temperature was approached by cooling. The peak temperature was maintained at a temperature greater than that of the test temperature by 50 °C. The  $K_I$  was calculated using Eqs. (2) and (3) [26].

$$K_I = \frac{P_0}{BW^{1/2}} f\left(\frac{a}{w}\right) \quad (2)$$

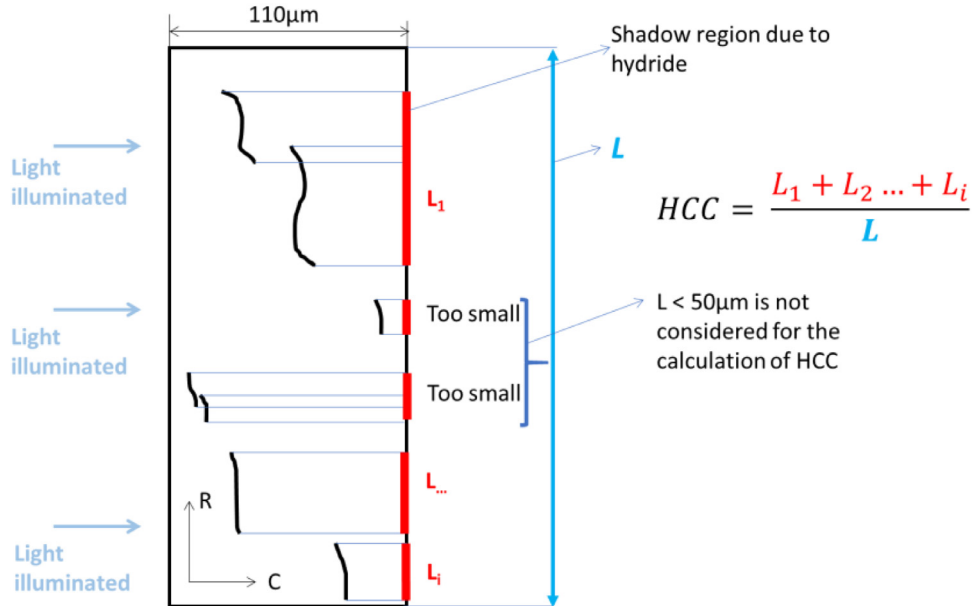


**Fig. 3.** Illustration of calculation of HCC in the PT [13]

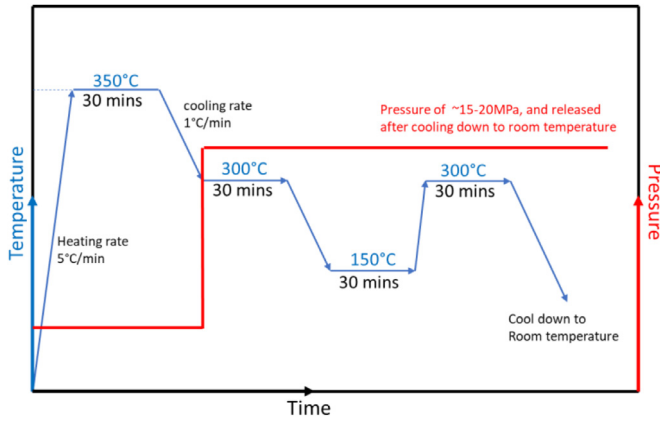


**Fig. 2.** A schematic showing Pressure and temperature vs. Time during the reorientation treatment of the pressure tube.

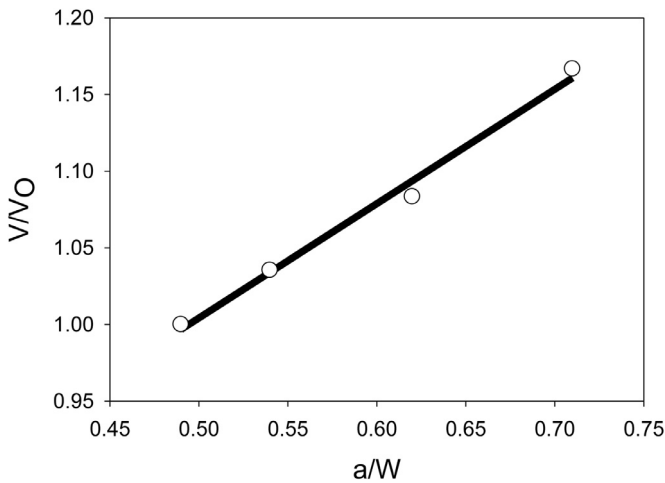


**Fig. 4.** Plot showing variation  $V/V_0$  with  $a/W$  for radial hydrided samples.

where  $P_Q$  = applied load (N),  $B$  = sample thickness (m),  $W$  = sample width (m),  $a$  = crack length (m) and

$$f\left(\frac{a}{w}\right) = \frac{\left[2 + \frac{a}{w}\right] \left[0.886 + 4.64\frac{a}{w} - 13.32\left(\frac{a}{w}\right)^2 + 14.72\left(\frac{a}{w}\right)^3 - 5.6\left(\frac{a}{w}\right)^4\right]}{\left(1 - \frac{a}{w}\right)^{3/2}} \quad (3)$$

The DHC test was carried at constant load, such that the initial  $K_I$  for DHC tests was maintained around 20 MPa.m<sup>1/2</sup>. Three K-type thermocouples were mounted to monitor and control the temperature with in  $\pm 1$  °C. Direct current potential drop (DCPD) technique using the constant current source of 6A was used to monitor the crack growth during the DHC tests. Platinum wire of 0.2mm diameter was welded to crack mouth to record the voltage drop across the crack front. The variation  $V/V_0$  with  $a/W$  is shown in Fig. 4 and found to be linear. The samples after testing were pulled apart and images were taken using the stereo microscope. The stereo images were analysed to obtain the initial and final crack lengths using the 9-point measurement. The initial fatigue pre-crack symmetry was qualified by the ASTM standard E1820 [37], where the nine measurement of the crack size should not differ by 0.05B of the measured average size using the nine measurements. Most of the pre-crack in the specimens for the DHC test met the above criteria except for one sample where one of the

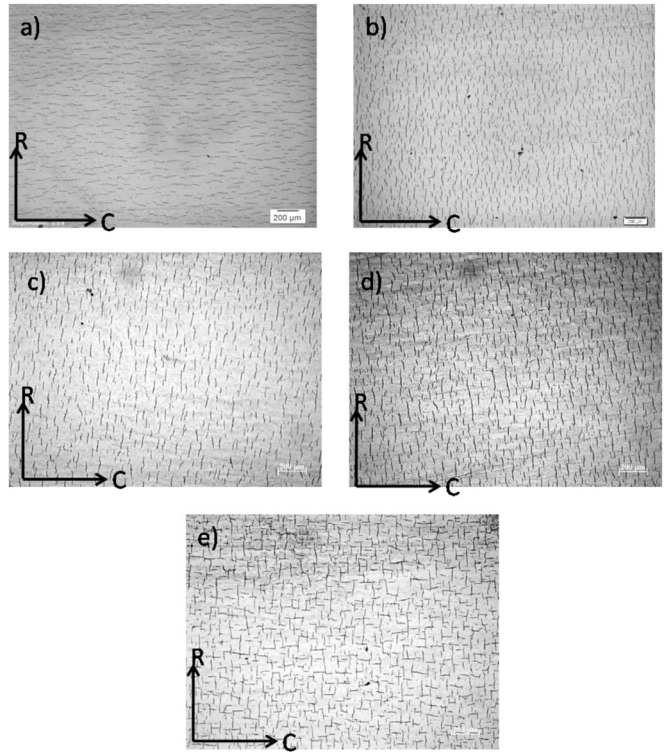


**Fig. 5.** A typical micrograph of the tube containing 70wppm hydrogen a) before reorientation treatment, b) after the re-orientation procedure, c) post test at 200 °C, d) post test at 225 °C and e) post-test at 250 °C. Dark lines are trace of hydrides. R and C refer to the radial and circumferential directions of the PT, respectively.

Reading did not meet the criteria by few microns. The average  $V_{DHC}$  was determined by dividing the net crack growth with the duration of cracking time, as no incubation was observed. Also, instantaneous  $V_{DHC}$  was determined using DCPD output during the DHC test [14].

### 3. Results

#### 3.1. Hydride micrograph and HCC

The optical micrograph of the as hydrided Zr-2.5Nb PT material containing 70wppm hydrogen is shown in the Fig. 5. From the Fig. 5(a) it is seen that hydrides are oriented along the circumferential-axial direction of the PT to form circumferential hydrides in the as hydrided condition. The tube was subjected to stress re-orientation test as explained in the Section 2.2. The optical micrograph of the tube after the stress re-orientation test is shown in the Fig. 5(b). The hydrides completely precipitated in the radial-axial direction to form the radial hydrides after the stress re-orientation treatment. The CCT samples were fabricated from the as hydrided PT spool to estimate the  $V_{DHC}$  for the circumferential hydrided samples and the CCT samples were fabricated from the stress re-oriented PT section to estimate the  $V_{DHC}$  for the radial hydrided samples. The CCT samples containing radial hydrides were analysed for the HCC. The mean HCC values for the radial hydrided CCT samples were found to be ~0.80. The average length of radial hydride in the axial circumferential (AC) plane was found to be in the range of  $142 \pm 55 \mu\text{m}$  at room temperature. The solubility of the hydrogen during cooling (Terminal solid solubility during precipitation-TSSP) at the test temperatures was calculated using Eq. (4) [38] and are 35, 48 and 65wppm at 200, 225, and 250 °C,

respectively.

$$\begin{aligned} C^{TSSD}_H &= 8.080 \times 10^4 \times \exp[-34520/RT] TSSD \\ C^{TSSP}_H &= 2.473 \times 10^4 \times \exp[-25840/RT] TSSP \end{aligned} \quad (4)$$

where  $C^{TSSD}_H$  and  $C^{TSSP}_H$  stands for the hydrogen concentration during dissolution and precipitation of the hydride respectively,  $R$  is the gas constant 8.3144 J/mol.K and  $T$  is the temperature in K.

The hydride micrograph post DHC test for radial hydrided samples, where peak temperatures were in the range of 250–300 °C, is shown in Fig. 5(c-e). From the post test hydride micrograph in the Fig. 5(c-e), it is evident that no reorientation back to circumferential hydride was observed for the peak temperatures of 250 and 275 °C. Partial reorientation to circumferential hydride is observed in the samples for peak temperature of 300 °C and hence mixed orientation is observed in those samples.

### 3.2. $V_{DHC}$ for the radial & circumferential hydrided samples

DHC tests for the circumferential hydrided and radial hydrided samples of Zr-2.5Nb were performed in the temperature range of 200–250 °C using CCT samples. The typical variation of the load, temperature and DCPD with time (duration of the test), is plotted in the Fig. 6 at 200, 225 and 250 °C for both the radial hydrided and circumferential hydrided samples. The DCPD signal for the radial hydrided sample is varying non-linearly with the time duration of the applied load indicating variable crack propagation rates at 200 °C and 225 °C (Fig. 6(a, b)) whereas the DCPD signal increases linearly with time at 250 °C suggesting a constant crack propagation rate (Fig. 6(c)). For the circumferential hydrided sample, the DCPD signal increased linearly with time during the entire duration of DHC test at all test temperatures (Fig. 6(a-c)). This indicates a constant rate of crack propagation for the circumferential hydrided samples in the temperature range of 200–250 °C. Therefore, the  $V_{DHC}$  at any test temperature and between the initial and final  $K_I$  imposed during the test will be equal to average  $V_{DHC}$  for the circumferential hydrided samples.

The variation of the  $V_{DHC}$  for the radial hydrided and circumferential hydrided sample with  $K_I$  in the temperature range 200–250 °C is shown in the Fig. 7. For the radial hydrided samples tested at 200 and 225 °C, the  $V_{DHC}$  was found to be increasing with the increase in applied  $K_I$  (Fig. 7(a,b)). However, for the test temperature of 250 °C, the  $V_{DHC}$  was found to be constant with the increase in  $K_I$  (Fig. 7(c)). A similar result of constant  $V_{DHC}$  was observed with the increase in the  $K_I$  for the circumferential hydrided samples in the temperature range of 200–250 °C as shown in the Fig. 7(a-c).

The average  $V_{DHC}$  velocities for both the radial and circumferential hydrided samples are given in the Table 3 along with the summary of the DHC test performed in this study. The plot of the average  $V_{DHC}$  with inverse of the temperature ( $1/T$ ) is shown in the Fig. 8(a). The average  $V_{DHC}$  for the circumferential hydride was varying linearly with  $1/T$  and for the radial hydride the average  $V_{DHC}$  displayed a non-linear variation with  $1/T$ . The theoretical ratios of  $V_{DHC}$  in presence and in absence of the radial hydrides were calculated by the  $1/(1-HCC)$  at test temperature (HCC values in Table 4) at 200–250 °C. The theoretical and the experimentally determined ratio of  $V_{DHC}$  in presence and in absence of the radial hydrides are shown in the Fig. 8(b).

### 3.3. Fractography

The stereo-fractographs of the surfaces of the broken samples containing radial hydride and circumferential hydride tested at 200, 225 and 250 °C are shown in the Fig. 9. The surfaces of the both the radial and circumferential hydride samples display three distinct regions. The regions are fatigue pre-crack, DHC region and

**Table 3**

Summary of the DHC tests for the radial hydrided and circumferential hydrided samples of Zr-2.5 Nb PT material. RH and CH are nomenclatures for radial hydrided sample and circumferential hydrided sample, respectively.

Sample id	Temperature, °C	Cracking Time	$K_I$ , MPa.m <sup>1/2</sup>	Average $V_{DHC}$ m/s
Peak	Test	Initial	Final	
RH-36	250	200	26.47	22.19 45.16 <b>3.05E-08</b>
RH-06	250	200	23.57	18.83 29.44 <b>2.5E-08</b>
RH-25	250	200	30	21.11 29.15 <b>1.87E-08</b>
RH-03	275	225	17.24	22.10 41.84 <b>4.12E-08</b>
RH-23	275	225	18.67	20.20 44.30 <b>4.76E-08</b>
RH-12	275	225	18	19.25 40.81 <b>3.89E-08</b>
RH-07	300	250	10	20.39 30.48 <b>5.11E-08</b>
RH-38	300	250	10	18.27 26.95 <b>5.36E-08</b>
RH-05	300	250	10	18.55 27.12 <b>5.37E-08</b>
CH-01	250	200	48	20.80 28.26 <b>9.38E-09</b>
CH-04	250	200	48	21.15 29.35 <b>1.05E-08</b>
CH-02	275	225	20	18.70 25.07 <b>2.06E-08</b>
CH-06	275	225	20	19.25 26.7 <b>2.44E-08</b>
CH-03	300	250	10	17.98 25.01 <b>4.69E-08</b>
CH-05	300	250	10	17.56 24.67 <b>4.36E-08</b>

post DHC region. The crack growth for the radial hydrided samples was more than the crack growth of the circumferential hydride samples corresponding to the  $V_{DHC}$  observation as stated above. However, the DHC fractured surface of the radial hydrided samples was similar to the DHC fractured surface of the circumferential hydrided samples. The following observations are made:-

- (1) The crack tunnelling at 200 °C and 225 °C was observed for radial hydride samples, whereas the circumferential hydride samples had uniform crack growth across the thickness of the sample at 200, 225 and 250 °C.
- (2) The radial hydrided sample tested at 250 °C had uniform crack growth over the range of stress intensity factor imposed during the test and was similar to the circumferential hydrided sample.

### 3.4. Hydride fracture zone

The contour plot of the  $\sigma_{yy}$  at 30MPa.m<sup>1/2</sup> is shown in the Fig. 10. Contour plots of von Misses stress showing the plastic zone around the crack tip for the  $K_I$  in the range of 12–30 MPa.m<sup>1/2</sup> are shown in the Fig. 11. Contour plots of  $(\sigma_{yy}-\sigma^h)$  stress showing hydride fracture zone, considering the hydride compressive stress field present throughout the region, at different  $K_I$  near to the crack tip are shown in the Fig. 12. In these figures, the hydride fracture zone is the region where the stresses are more than that of the fracture stress of the hydride, i.e. 600 MPa [34, 36]. From the Fig. 12, it is evident that the hydride fracture zone volume for unit thickness is increasing with the increase in  $K_I$ . The variation of hydride fracture zone and plastic zone volume with  $K_I$  is shown in the Fig. 13. From the Fig. 13, the hydride fracture zone volume is comparable to the plastic zone volume till 12MPa.m<sup>1/2</sup> and above 12MPa.m<sup>1/2</sup>, it is smaller than that of the plastic zone volume.

## 4. Discussion

### 4.1. Hydride orientation at DHC temperature

During the DHC test, the test temperature is achieved by cooling from a peak temperature [26]. In the present study, the peak temperature was 50 °C more than that of the test temperature i.e. 300, 275, and 250 °C for the test temperature of 250, 225 and 200 °C, respectively. Since the test temperature has been achieved by cooling, the maximum solubility of hydrogen in Zr-2.5Nb PT material is calculated using the Eq. (4) at the test temperature of 200, 225 and 250 °C. The maximum solubility was found to be 35, 48 and

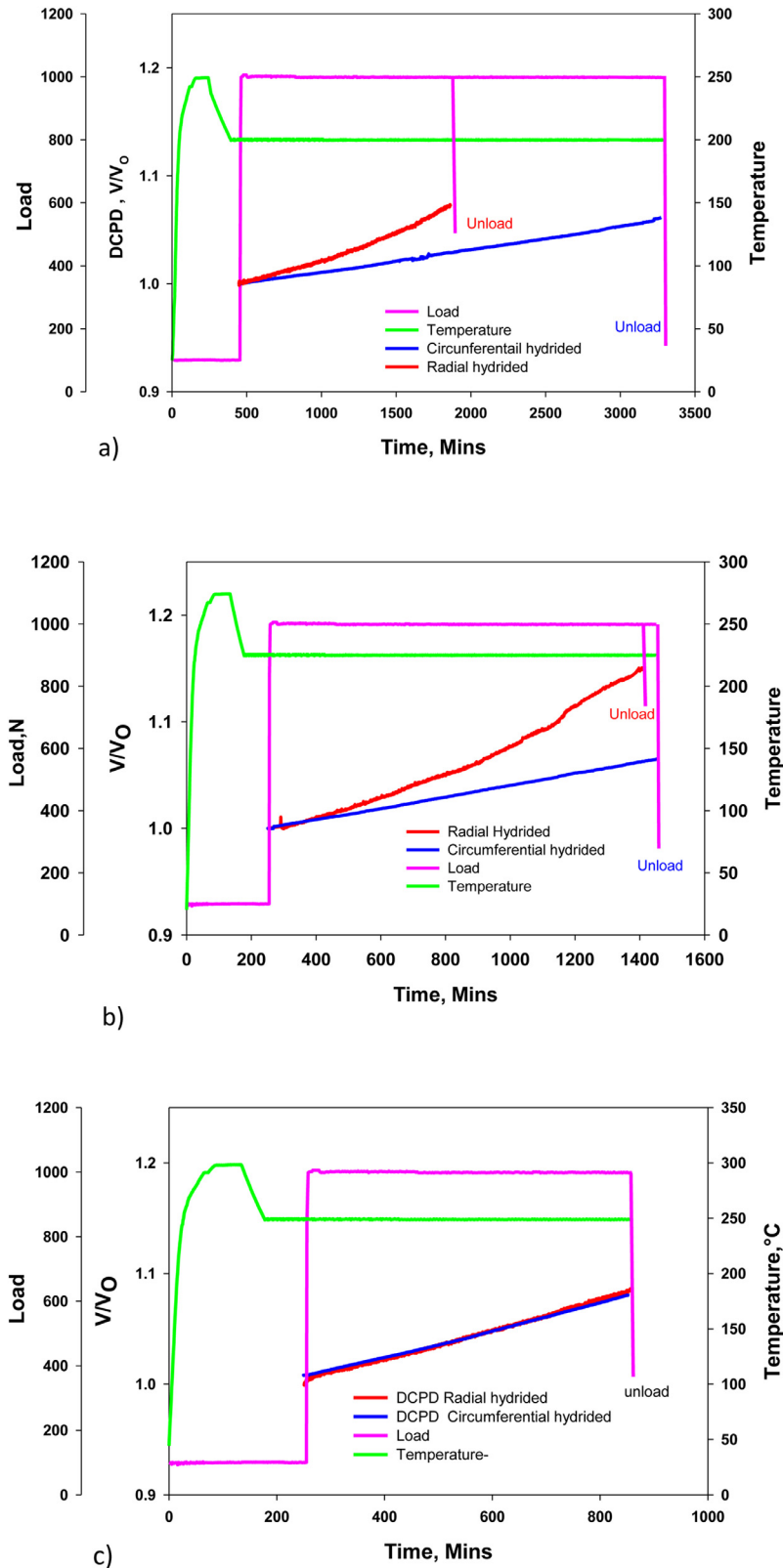


**Fig. 6.** Plot of the DCPD, load and sample temperature against time obtained during the DHC test carried out at a) 200, b) 225 and c) 250 °C.

65wppm at 200, 225, and 250 °C, respectively. The actual solid solubility of hydrogen will be the lower value among the TSSD at peak temperature and TSSP at the DHC test temperature. The peak temperature was chosen about 50 °C higher than the DHC test temperature and in such case both the TSSD at peak tempera-

ture and TSSP at DHC test temperature are comparable. Hence, out to total 70 wppm of hydrogen 35, 22 and 5wppm of hydrogen are expected to be present as undissolved hydrides at 200, 225 and 250 °C, respectively. Therefore, in the radial hydrided samples at the test temperature, the length of radial hydride will shrink with

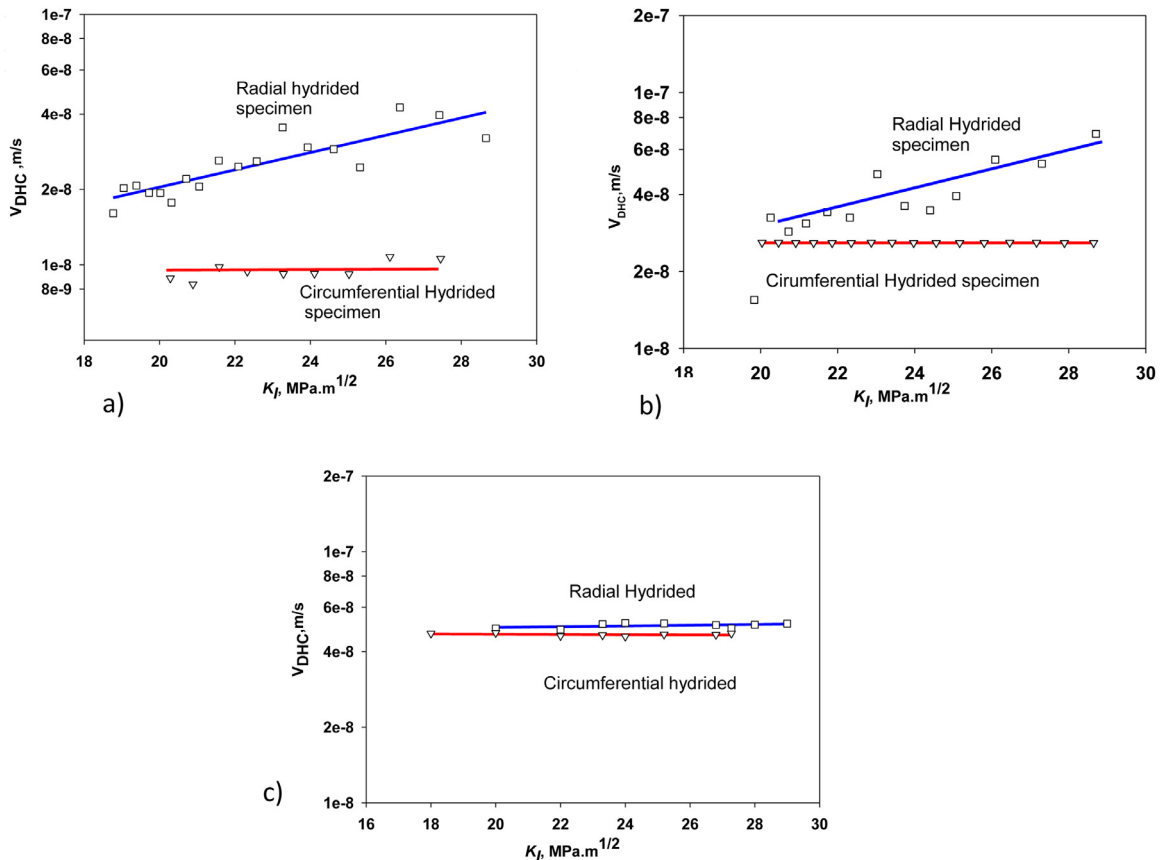


**Fig. 7.** Plot of  $V_{DHC}$  with  $K_I$  for Radial hydride and circumferential hydrided sample at a) 200 °C, b) 225 °C and c) 250 °C.

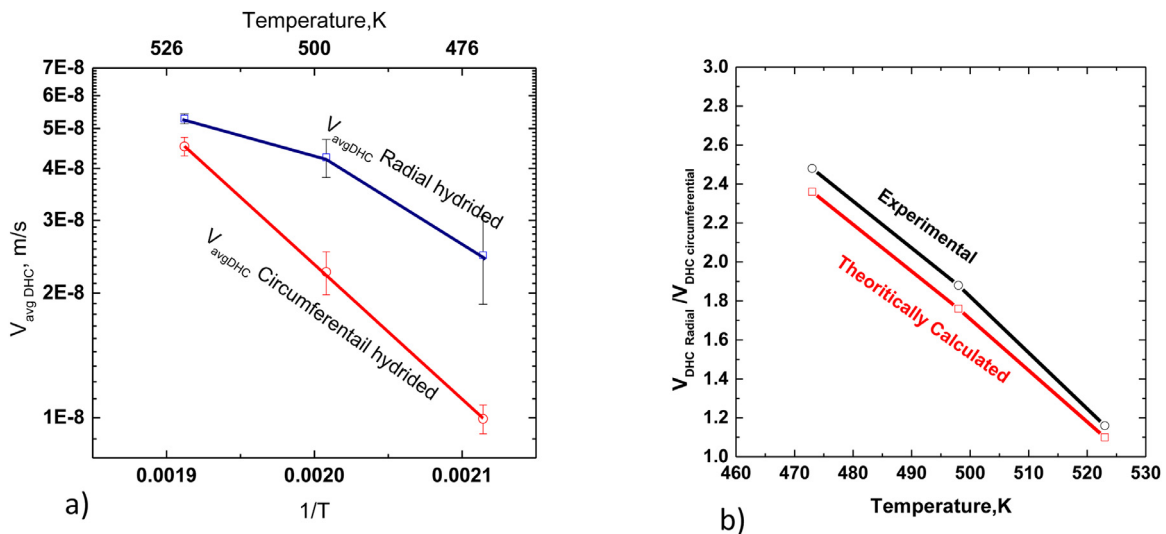


**Fig. 8.** Plot of a) average  $V_{DHC}$  with inverse of the test temperature for the radial hydrided and circumferential hydrided samples and b) theoretically predicted and experimentally determined ratio of the DHC velocity of radial and circumferential hydrided samples with temperature.

**Table 4**  
Estimated radial hydride length in the AC plane of radial hydrided sample and corresponding HCC at the test temperatures

Temperature, °C	Estimated Radial Hydride Length in AC Plane (μm)	Estimated HCC
25	142	0.8
200	100.82	0.576
225	78	0.44
250	10	-

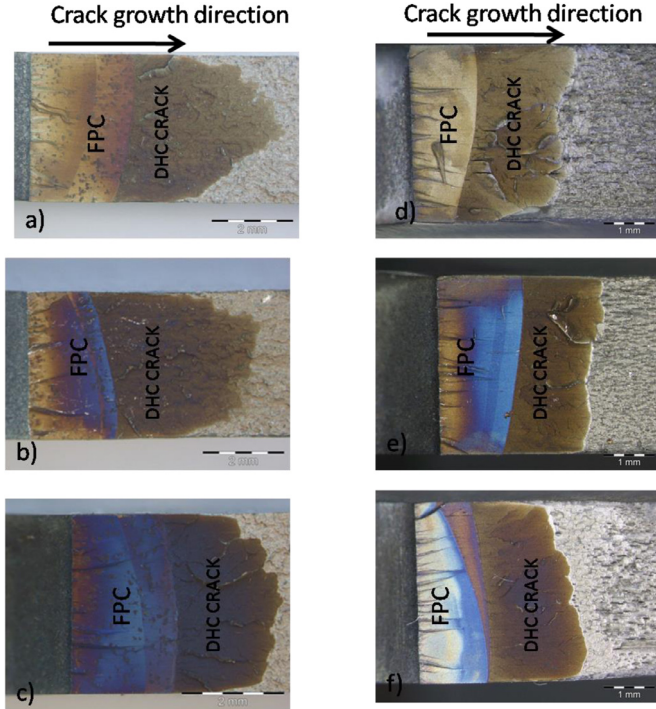


**Fig. 9.** Fractographs showing the fatigue pre-crack (FPC) and DHC crack for the radial hydrided (a,b,c) and circumferential hydrided (d,e,f) CCT samples subjected to DHC test at 200 °C (a & d), 225 °C (b & e) and 250 °C (c & f), respectively.

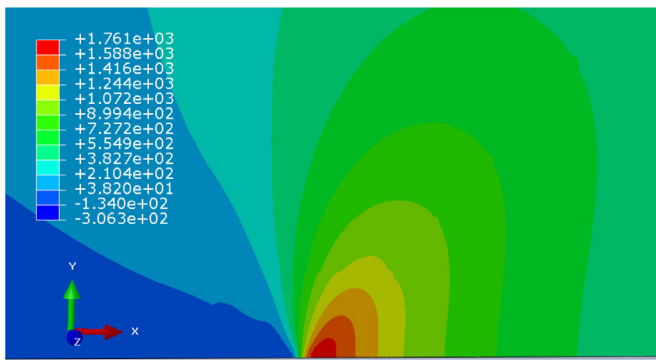


**Fig. 10.** Contour plot of  $\sigma_{yy}$  around the crack tip corresponding to a  $K_I$  of  $30 \text{ MPa.m}^{1/2}$ . The stress values are in MPa in the legend. The crack growth direction is from left to right.

increase in the temperature. This leads to decrease in HCC with increase in the test temperature. The average length of the radial hydride on Axial-Circumferential (AC) Plane and the HCC could be estimated at the test temperature by considering isotropic dissolution of hydrides with temperature and is provided in [Table 4](#). However, one should note that the above method to calculate HCC at test temperature should be only considered when either completely radial or circumferential orientation is present. In case of mixed hydride sample, as used by Grigoriev et al. [27] in Zr-2 clad tubes, a competition in dissolution tendency of radial and circumferential hydride may takes place and deviation from isotropic dissolution is expected.

#### 4.2. Effect of temperature on post DHC test hydride orientation

The post DHC test hydride micrograph ([Fig. 5\(c-e\)](#)) indicates memory effect of hydrides in Zr-2.5Nb alloys [39, 40], where hydride prefers to precipitate at the dislocation networks present at the pre-existing radial hydride locations. These micrographs indicate the importance of the selection of the peak temperature in the DHC test for radial hydride samples. In general, peak temperature is selected such that TSSP condition exists at the test temperature. However, in case of radial hydrided samples, a higher peak temperature may cause partial reorientation as shown in [Fig. 5\(e\)](#) for a test temperature where TSSD (Peak temperature) > TSSP (test temperature). Therefore, selection of the peak temperature is of utmost importance when the DHC test of radial hydrided samples is being carried out and the peak temperature should be selected in a such a way to ensure the presence of radial hydrides at the DHC test temperature.

#### 4.3. Difference in average $V_{DHC}$ for radial and circumferential hydride samples

The variation of the average  $V_{DHC}$  velocity with inverse of temperature is shown in [Fig. 8\(a\)](#). The average  $V_{DHC}$  for circumferential hydrided samples was found to be linearly increasing with increase in the test temperature. In case of the radial hydrided samples, the average  $V_{DHC}$  was found to be increasing non-linearly with increase in the test temperature. The ratio of the average  $V_{DHC}$  of radial hydrided samples and circumferential hydrided samples at 200 and 225 °C was 2.5 and 1.85, respectively. However, at 250 °C, the average  $V_{DHC}$  for the radial and circumferential hydrided samples was found to be similar. The result obtained at 200 and 225 °C in the present study is in contrast with that of the work of Grigoriev et al. [27] on the DHC behaviour of Zr-2 clad tubes containing re-oriented radial hydrides where it was reported that the presence of radial hydrides does not affect the DHC behaviour. However, in the work of Grigoriev et al. [27] both the circumferential and radial hydrides were present. Also, as mentioned in the [Section 4.1](#) for

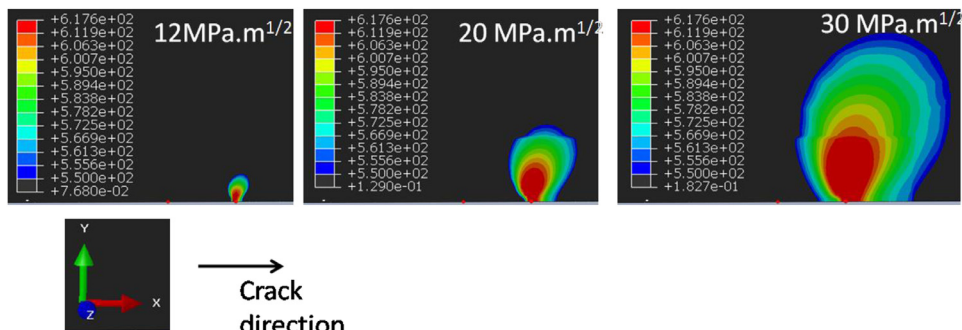


**Fig. 11.** Contour plot of von Misses stress around the crack tip showing plastic zone size for  $K_I$  in the range of  $12\text{--}30 \text{ MPa.m}^{1/2}$  at  $200^\circ\text{C}$ . The crack growth direction is left to right. The stress values are in MPa in the legend.

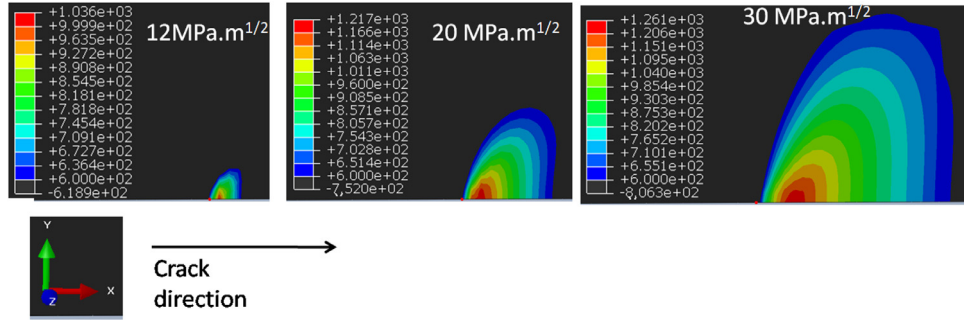


**Fig. 12.** Contour plot of  $\sigma_{yy} - \sigma^h$  around the crack tip showing hydride fracture zone volume for unit thickness with  $K_I$  in the range of 12–30 MPa.m<sup>1/2</sup> at 200 °C. The crack growth direction is left to right. The stress values are in MPa in the legend.

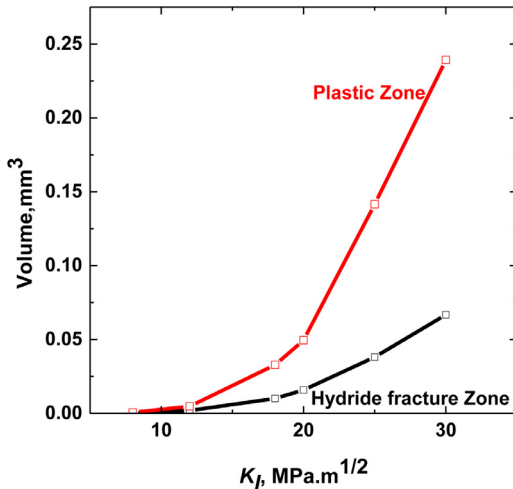


**Fig. 13.** Variation of hydride fracture zone and plastic zone volume for unit thickness with  $K_I$  at 200 °C.

mixed hydride orientations, the peak temperature employed would be sufficient to dissolve all the radial hydrides back into the solution. This is similar to the results obtained at 250 °C for the radial hydrided sample, where no pre existing radial hydride is present at the test temperature.

Generally, the variation of the  $V_{DHC}$  with temperature is reported to exhibit an Arrhenius type relationship [22]. The Activation energy associated with the  $V_{DHC}$  for the circumferential hydride sample could be represented by the Eq. (5) The activation energy associated with the  $V_{DHC}$  was found to be ~54.4 kJ/mol for circumferential hydrided samples, which is similar to the values reported in the literatures [15, 25, 30, 41]. However, similar treatment could not be applied for the average  $V_{DHC}$  for the radial hydrided samples.

$$V_{DHC} = 0.087 \exp(-54.4 \text{K}/\text{RT}) \text{CircumferentialHydrided} \quad (5)$$

The post test hydride micrographs for the circumferential hydrided and radial hydrided specimens subjected to tests at 200 °C are shown in Fig. 14. A total of 3 no.'s micrographs of the radial hydrided specimens and 2 no.'s micrographs of the circumferential hydrided specimens were analysed to check for the validity of the observation. The Micrograph of circumferential hydrided specimen (Fig. 14(a)) revealed that the crack propagation is planer in nature. However, the micrograph of radial hydrided specimen revealed that the crack growth is facilitated by the pre-existing radial hydrides and at initial  $K_I$ , the crack path is planer and at final  $K_I$ , the crack path is zigzag. The bridging of these pre-existing radial hydrides provides a shorter path for the crack growth at temperatures of 200 and 225 °C as compared to the circumferential

hydrided samples. The presence of the pre-existing radial hydrides is responsible for the increased average  $V_{DHC}$  at 200°C and 225 °C. For the DHC test at 250 °C, for both the circumferential and radial hydrided cases, hydrogen was present nearly in the solution, which resulted in similar  $V_{DHC}$  for both the circumferential and radial hydrided samples at 250 °C.

An observation is to be noted from the Table 4 that the length of the pre-existing radial hydride in AC plane is more than the critical hydride length of 15–20  $\mu\text{m}$  required for the cracking in the Zr-2.5Nb alloys [15, 30, 42–44]. Therefore, one possibility is that when the pre-existing radial hydride is connected by the radial hydride precipitated near to crack tip, the length of radial hydride fractured would be more as compared to the critical crack length observed during DHC. However, joining of the pre-existing radial hydrides in crack growth direction i.e. AC plane is not sufficient condition for crack propagation. Another important factor associated with crack propagation in the radial hydrided samples is the HCC. The HCC determined using hydride micrograph along the RC plane of the tube defines connectivity of hydrides across the thickness of the sample. For DHC crack propagation, radial hydrides should nearly cover entire the crack front. Therefore, the amount of hydrogen required to cover the crack front would be less in presence of the pre-existing radial hydrides as compared to the circumferential hydrided sample. The amount of hydrogen required to cover the crack surface will depend on the HCC of the sample. Hence, the average  $V_{DHC}$  of the radial hydrided samples is expected to be higher as compared to that of the circumferential hydrided samples (as HCC for circumferential hydride sample is negligible). For the radial hydrided samples, the estimated HCC (Table 4) at 200 and 225 °C is 0.56 and 0.44, respectively. As mentioned earlier, the hydride length in the AC plane is more than the critical hydride length. Therefore, bridging of the radial hydride in the thickness plane (RC plane) would be the rate controlling step and hence the HCC at test temperature would be a rate controlling parameter in case of the radial hydrided samples at 200 and 225 °C. This will be discussed in details in Section 4.6.

At 250 °C, hydrogen is nearly in the solid solution for both the radial hydrided and circumferential hydrided sample. Hence, HCC is negligible. Therefore, negligible difference was observed in the average  $V_{DHC}$  for both the radial and circumferential hydrided samples. From the above discussion it is evident that the HCC is an important parameter in affecting the average  $V_{DHC}$  in case of the radial hydrided samples at 200 and 225 °C.

From the above results it could be inferred that the higher  $V_{DHC}$  is due to pre-existing radial hydrides in radial hydrided samples at the test temperatures. However, the higher average  $V_{DHC}$  of the radial hydrided specimens observed at lower temperature is not likely to affect the average  $V_{DHC}$  at reactor operating temperature of 300 °C unless hydrogen concentration is large enough to ensure presence of radial hydrides at the reactor operating condition.

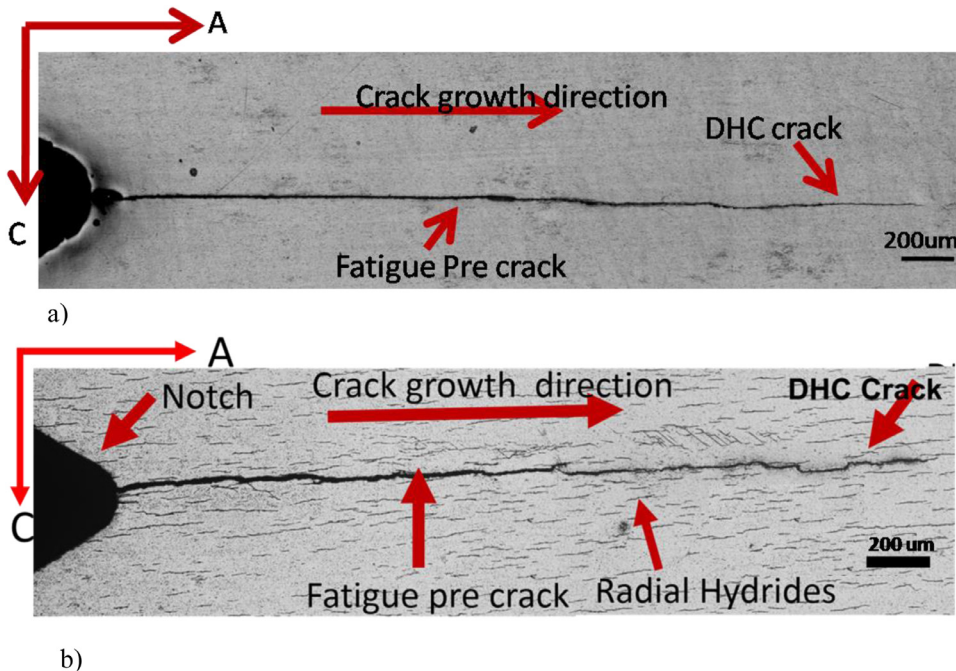


**Fig. 14.** Optical micrograph of the axial circumferential plane of the a) Circumferential hydrided and b) Radial hydrided sample subjected to DHC test at 200 °C. Radial Hydrided specimen showing joining and crack propagation through pre-existing radial hydride cluster. At initial  $K_I$  crack path is planer and at final  $K_I$  the crack path is zigzag.

Hence it is important that hydrogen concentration and hydride orientation be monitored at regular interval and to ensure that hydrogen concentration is lower than TSSP in the main body of the pressure tube.

#### 4.4. Effect of $K_I$ on $V_{DHC}$ for radial hydrided and circumferential hydrided samples

The DHC has been implicated as one of the insidious degradation mechanisms in CWSR Zr-2.5Nb PT material. It involves migration of hydrogen up the hydrostatic stress gradient to the region of stress concentration. Once the terminal solid solubility of hydrogen is exceeded the brittle hydride platelet (radial hydride) nucleates perpendicular to the tensile stress, grows to a critical size and then the crack grows by the fracture of critical hydride and matrix ligament [45]. The above process repeats over and over during the DHC. In typical  $V_{DHC}$  vs.  $K_I$  plot [15], the  $V_{DHC}$  was found to be independent of the  $K_I$  for  $K_I$  sufficiently greater than the threshold  $K_I$  ( $K_{IH}$ ). The values of the  $K_{IH}$  lies in the range of 8–11 MPa·m<sup>1/2</sup> [30] for an un-irradiated Zr-2.5Nb PT and 4–5 MPa·m<sup>1/2</sup> [41] for an irradiated Zr-2.5Nb PT. The reason for constant  $V_{DHC}$  with  $K_I$  was explained on the basis of the critical hydride length and plastic zone size. Many researchers [30, 42, 43] have shown that for the Zr-2.5Nb PT material, the critical hydride length is constant if the plastic zone size is greater than the critical hydride length. This constant critical hydride length is further correlated to the crack growth in each DHC step [15, 43, 44]. From Fig. 13, it can be seen that the hydride fracture zone volume is either comparable or smaller than the plastic zone. It could be observed that the hydride fracture zone volume is sufficiently large to accommodate the critical hydride length for  $K_I > 12 \text{ MPa} \cdot \text{m}^{1/2}$ . Since, the hydride fracture zone is the region having stresses greater than the fracture stress of the constrained hydride of the critical length, the hydride fracture zone would be a better parameter to correlate the DHC phenomena. The above stated mechanism and  $V_{DHC}$  behaviour of Zr alloys is for the Zr-matrix with no pre-existing radial hydrides at the test temperature. A result similar to the typical behaviour

of  $V_{DHC}$  with  $K_I$  [15] for the circumferential hydrided samples is obtained, which is independent to the  $K_I$  (Fig. 7(a-c)) in the temperature range of 200–250 °C.

From the above, it could be inferred that the hydride fracture zone is the region in which the hydrogen diffuses and on exceeding the TSSP, it leads to the precipitation of radial hydride. This radial hydride grows to a critical length and subsequently fractures, leading to the DHC crack propagation. The average length of the pre-existing hydride at test temperature of 200 °C and 225 °C is provided in the Table 4. From the table, it is observed that the length of the pre-existing radial hydride is greater than the critical hydride length required for the hydride fracture ahead of the crack tip [15, 30, 43]. Also, the hydride fracture zone volume (Fig. 13) is greater than the pre-existing hydride at the test temperatures (Table 4) for 20 MPa·m<sup>1/2</sup>. Based on the inter-platelet distance (Fig. 14(b)) in direction perpendicular and along hydride platelets, hydride fracture zone can accommodate a fraction or a complete hydride platelet of the pre-existing radial hydride at 200 and 225 °C, respectively at 20 MPa·m<sup>1/2</sup>.

A hydride platelet is comprised for several sub-platelets, especially in the case of radial hydrides where it comprises very small sub-platelet type configuration [46]. The pre-existing full or partial radial hydride platelet connected by the precipitated radial hydrides inside the hydride fracture zone would fracture in the radial hydrided samples at 200°C and 225 °C. We expect that the crack advancement will be limited to the connected hydride platelets inside the hydride fracture zone volume as the principal tensile stress wouldn't be sufficient to satisfy the fracture criteria outside the region. As the crack grows,  $K_I$  will increase, leading to increase in the hydride fracture zone volume. The number of the radial hydride inside hydride fracture zone would also increase with increase in the hydride fracture zone volume. This would increase the possibility of finding the least resistance path by joining of hydrides present on planes parallel to crack plane in thickness direction. Therefore, a higher crack growth rate is expected as the  $K_I$  is increasing. This hypothesis explains the increase in  $V_{DHC}$  with increase in  $K_I$ , which was observed for the radial hydrided samples

at 200 and 225°C as shown in the Fig. 7(a,b). Further details of the crack growth mechanism in presence of radial hydride is provided in Section 4.6.

The fraction or number of radial hydride accommodated by hydride fracture zone depends on the length and inter-platelet distance of hydride platelet at the test temperature. As the temperature is increasing the inter-platelet distance between the radial hydride will also increase. This will lead to sparse distribution of radial hydrides, leading to rare occurrence of interaction of pre-existing radial hydride with the hydride fracture zone volume. A similar case is expected for the radial hydrided sample at 250 °C. In this case the radial hydride length has been reduced to approx ~10μm and the inter-platelet distance would have also increased substantially. This has led to a constant  $V_{DHC}$  with  $K_I$  at 250 °C for the radial hydrided samples. From this we could infer that the pre-existing radial hydride length in the AC and RC plane as well as its distribution at the test temperature will affect the DHC behaviour with the  $K_I$ .

#### 4.5. Crack tunnelling during DHC

The crack tunnelling for samples in radial hydrided sample at 200 and 225 °C was observed as shown in the Fig. 9(a,b). In the literature crack tunnelling was observed for lower thickness samples or sample tested at the elevated temperatures [24, 42]. The crack tunnelling occurs when there is difference in the velocity at the centre and at the edge of the sample. Stress state at the crack tip governs the hydrogen diffusion in the DHC process [47, 48]. In the case of thin samples or samples tested at higher temperatures, the stress state transition occurs across the specimen thickness. Therefore, the occurrence of crack tunnelling is generally observed. However, in the case of the radial hydrided samples crack tunnelling may be getting accentuated because of the dependence of the velocity on  $K_I$  as shown in the Fig. 7(a,b). Another difference is the severity of the tunnelling was found to be increasing with that of the increase in the temperature for the lower thickness circumferential hydrided samples [24], which will not be applicable in this case as the all the samples used were of same thickness. However, from the fractograph (Fig. 9), the severity of tunnelling was decreasing with the increase in the temperature in case of the radial hydrided samples.

#### 4.6. Mechanism of DHC crack growth in presence of radial hydrides

The mechanism of DHC crack growth in the absence of pre-existing radial hydride is explained in Section 4.4. The major difference in the two cases is the presence of the radial hydride at the test temperature on the crack plane. To visualize the condition, a schematic of radial hydride traces (black lines) on the AC & RC planes of a specimen showing crack and hydride fracture zone for an applied  $K_I$  is shown in the Fig. 15(a). The region abcd in the Fig. 15(a) is showing corresponding hydride fracture volume for the applied  $K_I$ . An observation from the Fig. 9(a,b) and Fig. 14(b) is that the DHC crack propagates through the pre-existing radial hydride and there is a zig-zag crack path in both radial and axial directions depending on the probability of finding a nearest pre-existing radial hydride. With increase in HCC the probability of finding radial hydride in the hydride fracture zone is higher and hence the DHC velocity will be higher.

As mentioned earlier in the Section 4.3 that through thickness connectivity of hydride is represented by the HCC. As shown in schematic of hydride traces at 200 and 225 °C in Fig. 15(b,c), the hydride connectivity is more at the lower temperature and hence the HCC is higher. Therefore, based on the process explained above, the ratios of the  $V_{DHC}$  in presence and in absence of the radial hydrides should be theoretically equal to  $1/(1-HCC)$ . The theoretical

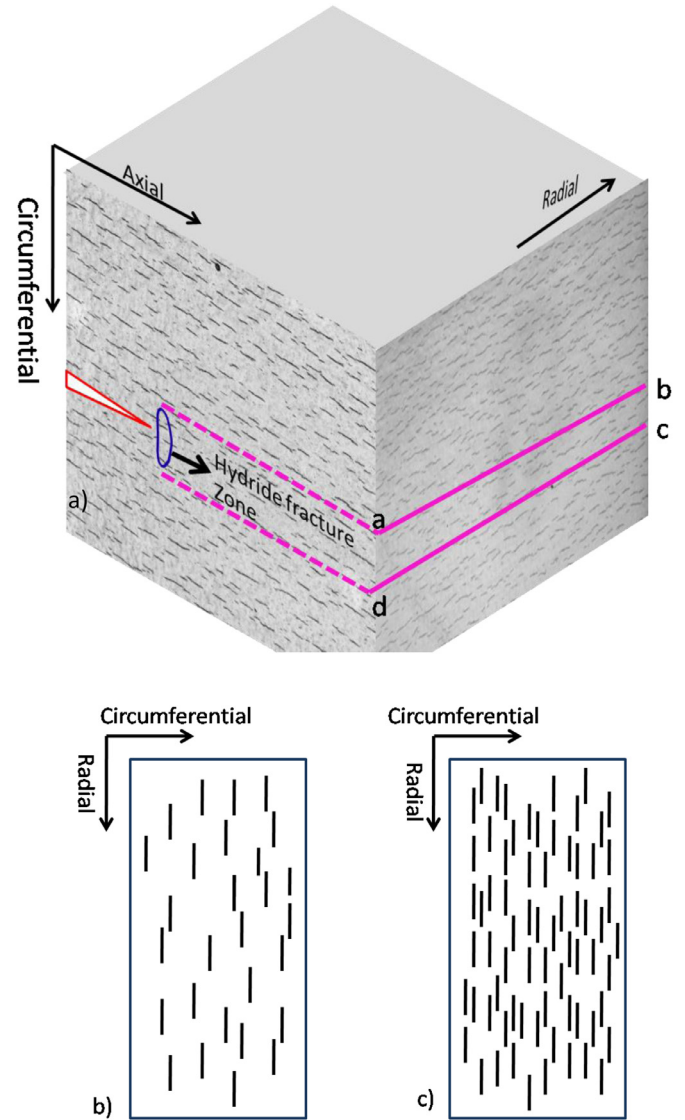


**Fig. 15.** Schematic of radial hydride traces (black lines) in a) AC & RC Plane of specimen showing crack and hydride fracture zone for a applied  $K_I$  test, b) RC plane at 225 °C, and c) RC Plane at 200 °C. The Region abcd showing the width of the corresponding hydride fracture zones along RC plane for the applied  $K_I$ .

ratios of  $V_{DHC}$  in the presence and absence of the radial hydrides were calculated by the HCC (Table 4) at 200 and 225 °C and shown in the Fig. 8(b) were 2.35 and 1.78 at 200 and 225 °C, respectively. These values are slightly less as compared to the experimental observed values of 2.5 and 1.85 at 200 and 225 °C, respectively. This may be because of considering an isotropic dissolution of the hydride platelets for calculating the HCC at the test temperature and enhanced hydrogen diffusion due to the interaction of local stress field of radial hydride platelets with the global stress gradient imposed by the crack. However, the theoretical treatment  $V_{DHC}$  for radial hydrided sample is in broad agreement with the results obtained in the tests.

Also, the zig-zag nature of the crack path is observed at higher  $K_I$ , suggesting, DHC crack propagation in presence of pre-existing radial hydride is not limited to a plane but to a set of parallel planes. Another observation is the increase of the  $V_{DHC}$  with increase in  $K_I$ .

To explain the above a schematic of the radial hydride trace on AC and RC plane with the hydride fracture zone is shown in the Fig. 16. The short black colour lines are the traces of pre-existing

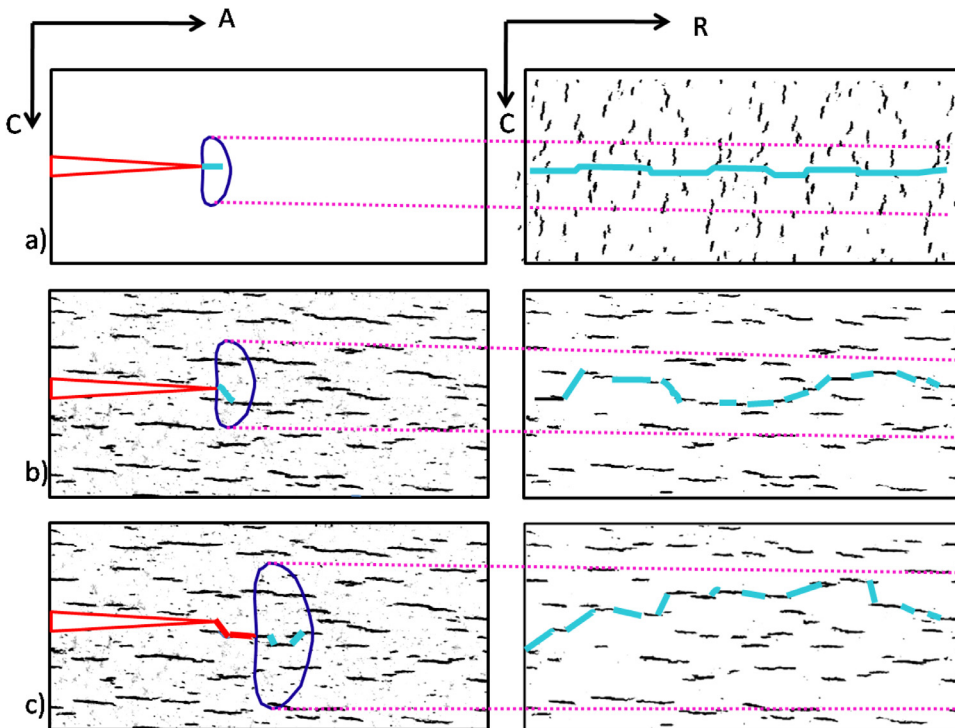


**Fig. 16.** Schematic showing Crack (red lines), hydride traces (black lines) in axial circumferential and radial-circumferential planes with hydride fracture zone (region bound within blue loop) and corresponding region in radial circumferential plane (marked by pink lines in Radial circumferential plane). In a) the planar crack path for circumferential hydride, zigzag crack path at b) initial  $K_I$  and c) final  $K_I$  is shown. (For interpretation of the references to colour in this figure legend, the reader is referred to the web version of this article.)

hydrides and the thicker cyan colour lines (RC Plane) are the traces of radial hydride precipitated by the DHC process, which bridges the pre-existing radial hydrides and leading to crack propagation. From the Fig. 16(a), the traces of the circumferential hydride (black lines) in RC plane could be seen. At the test temperature, the hydrogen will start diffusing inside the hydride fracture zone (region bound by blue loop) at the crack tip and on exceeding the TSSP condition, it will precipitate as radial hydride. This leads to a situation as shown in the Fig. 16(a), where the thickness of the sample (in RC plane) is being nearly covered by radial hydride of critical length (cyan) and hence leading to through thickness crack propagation. Whereas from the Fig. 16(b), when the pre-existing radial hydride is present, the zig-zag crack path along the radial direction is present due to bridging of the pre-existing hydride on the parallel planes lying in between the hydride fracture zone height shown by the pink dotted parallel lines. The zig-zag nature of the crack in the axial direction in the AC plane is due to bridging of the nearest radial hydride inside the hydride fracture zone. Now as the crack propagates,  $K_I$  increases, which leads to increase in the hydride fracture zone size. This situation is shown in the Fig. 16(c), where the number of radial hydride inside the hydride fracture zone increases, leading to higher probability of finding radial hydrides on the parallel planes leading to higher  $V_{DHC}$  with increase in the  $K_I$ .

## 5. Conclusion

For the first time the DHC crack growth rate in presence of the radial hydrides in the Zr-2.5Nb PT material has been determined. The DHC velocities for the Zr-2.5Nb PT material containing 70wppm of the radial and circumferential hydrides were determined in the temperature range of 200–250 °C. From the above work, the following conclusions could be drawn.

- (1) The circumferential hydrides were successfully re-oriented to radial hydrides for the Zr-2.5Nb PT material consisting of 70wppm of hydrogen by performing thermal cycling using the setup especially made for this purpose and described under the experimental section. The metallographic examination of the hydrogen charged spools subjected to the stress re-orientation treatment using this setup, revealed formation of the radial hydrides with mean HCC of 0.8.
- (2) The average  $V_{DHC}$  for the radial hydrided sample was found to be 2.5 and 1.85 times that of the average  $V_{DHC}$  for the circumferential hydrided samples at 200 and 225 °C, respectively. At test temperature of 250 °C, the average  $V_{DHC}$  is comparable for both the radial and circumferential hydrided samples. The increase in the average  $V_{DHC}$  radial hydrided samples as compared to the circumferential hydrided samples is correlated to the presence of pre-existing radial hydride and their HCC at the test temperature.
- (3) The  $V_{DHC}$  for circumferential hydrided sample was independent of  $K_I$  in the temperature range of 200–250 °C. However, for radial hydrided sample the  $V_{DHC}$  was found to be increasing with that of the increase of  $K_I$  at 200° and 225°C. At 250°C the  $V_{DHC}$  was again found to be independent of the  $K_I$ . The increase of the  $V_{DHC}$  with  $K_I$  is probably due to the increase in hydride fracture zone volume, leading to the more number of the pre-existing radial hydrides accommodated within the hydride fracture zone.

## Declaration of Competing Interest

The authors declare that they have no known competing financial interests or personal relationships that could have appeared to influence the work reported in this paper.

## Acknowledgement

Authors are grateful to Dr. Madangopal Krishnan, Distinguished Scientist and Associate Director, Materials Group, BARC for his constant encouragement and invaluable support. Constant encouragement provided by Dr. S. Banerjee and Dr. R. K. Sinha former secretaries, Department of Atomic Energy, Mr. S. A. Bhardwaj former AERB Chairman, Dr. G. K. Dey, former Director, Materials Group and Mr. A. K. Balasubramanian, Director (T), NPCIL is acknowledged. Technical assistance provided by Mr. S. A. Chandanshiv and Mr. Pramod N. Madavkar in hydrogen charging is acknowledged. This work was funded by XII plan project No. XII-N-R&D2500.

## References

- [1] L. Bell, An improvement in creep resistance of Zr-2.5% Nb tubes, *J. Nucl. Mater.* 57 (3) (1975) 258–270.
- [2] B. Cheadle, C. Coleman, H. Licht, CANDU-PHW pressure tubes: their manufacture, inspection, and properties, *Nucl. Technol.* 57 (3) (1982) 413–425.
- [3] E. Ibrahim, B. Cheadle, Development of zirconium alloys for pressure tubes in CANDU reactors, *Can. Metall. Q.* 24 (3) (1985) 273–281.
- [4] D. Srivastava, G.K. Dey, S. Banerjee, Evolution of microstructure during fabrication of Zr-2.5 Wt pct Nb alloy pressure tubes, *Metall. Mater. Trans. A* 26 (10) (1995) 2707–2718.
- [5] D. Northwood, U. Kosasih, Corrosion and hydriding behavior of Zr-2.5 wt. pct Nb alloy nuclear reactor pressure tubing, *J. Mater. Energy Syst.* 4 (1) (1982) 3–15.
- [6] R.N. Singh, R. Kishore, S. Singh, T.K. Sinha, B. Kashyap, Stress-reorientation of hydrides and hydride embrittlement of Zr-2.5 wt% Nb pressure tube alloy, *J. Nucl. Mater.* 325 (1) (2004) 26–33.
- [7] D. Northwood, U. Kosasih, Hydrides and delayed hydrogen cracking in zirconium and its alloys, *Int. Met. Rev.* 28 (1) (1983) 92–121.
- [8] J. Dunn, B. Kakaria, J. Graham, A. Jackman, CANDU-PHW Fuel Channel Replacement Experience, *Atomic Energy of Canada Ltd.*, 1982.
- [9] E. Perryman, Pickering pressure tube cracking experience, *Nucl. Energy* 17 (2) (1978) 95–105.
- [10] C. Simpson, O. Kucpis, Hydride Reorientation and Fracture in Zr Alloys, *Zirconium in the Nuclear Industry*, ASTM STP, 1977.
- [11] R.K. Sharma, A.K. Bind, G. Avinash, R.N. Singh, A. Tewari, B. Kashyap, Effect of radial hydride fraction on fracture toughness of CWSR Zr-2.5% Nb pressure tube material between ambient and 300°C temperatures, *J. Nucl. Mater.* 508 (2018) 546–555.
- [12] R.K. Sharma, S. Sunil, B. Kumawat, R.N. Singh, A. Tewari, B. Kashyap, Influence of hydride orientation on fracture toughness of CWSR Zr-2.5% Nb pressure tube material between RT and 300°C, *J. Nucl. Mater.* 488 (2017) 231–244.
- [13] A.C. Wallace, G.K. Shek, O.E. Lepik, Effects of Hydride Morphology on Zr-2.5 Nb Fracture Toughness, *Zirconium in the Nuclear Industry: Eighth International Symposium*, ASTM International, 1989.
- [14] R.N. Singh, N. Kumar, R. Kishore, S. Roychowdhury, T.K. Sinha, B.P. Kashyap, Delayed hydride cracking in Zr-2.5 Nb pressure tube material, *J. Nucl. Mater.* 304 (2) (2002) 189–203.
- [15] L.A. Simpson, M.P. Puls, The effects of stress, temperature and hydrogen content on hydride-induced crack growth in Zr-2.5 Pct Nb, *Metall. Trans. A* 10 (8) (1979) 1093–1105.
- [16] S.-Q. Shi, M.P. Puls, Dependence of the threshold stress intensity factor on hydrogen concentration during delayed hydride cracking in zirconium alloys, *J. Nucl. Mater.* 218 (1) (1995) 30–36.
- [17] M.P. Puls, Assessment of aging of Zr-2.5 Nb pressure tubes in CANDU reactors, *Nucl. Eng. Des.* 171 (1) (1997) 137–148.
- [18] S.S. Kim, S.C. Kwon, Y. Suk Kim, The effect of texture variation on delayed hydride cracking behavior of Zr-2.5% Nb plate, *J. Nucl. Mater.* 273 (1) (1999) 52–59.
- [19] S.S. Kim, Y.S. Kim, KH in radial textured Zr-2.5%Nb pressure tube, *J. Nucl. Mater.* 279 (2) (2000) 286–292.
- [20] S.Q. Shi, G.K. Shek, M.P. Puls, Hydrogen concentration limit and critical temperatures for delayed hydride cracking in zirconium alloys, *J. Nucl. Mater.* 218 (2) (1995) 189–201.
- [21] S. Kim, The texture dependence of  $K_{IH}$  in Zr-2.5% Nb pressure tube materials, *J. Nucl. Mater.* 349 (1) (2006) 83–95.
- [22] J. Ambler, Effect of Direction of Approach to Temperature on the Delayed Hydrogen Cracking Behavior of Cold-Worked Zr-2.5Nb, *ASTM International*, 1984.
- [23] D. Yan, R. Eadie, Calculation of the delayed hydride cracking velocity vs. K I curve for Zr-2.5 Nb by critical hydride cluster length, *J. Mater. Sci.* 37 (24) (2002) 5299–5303.
- [24] S. Sunil, A.K. Bind, H. Khandelwal, R.N. Singh, J.K. Chakravarthy, Effect of specimen thickness on DHC velocity for Zr-2.5 Nb alloy pressure tube material, *J. Nucl. Mater.* 467 (2015) 373–382.
- [25] R.N. Singh, S. Roychowdhury, V.P. Sinha, T.K. Sinha, P.K. De, S. Banerjee, Delayed hydride cracking in Zr-2.5 Nb pressure tube material: influence of fabrication routes, *Mater. Sci. Eng. A* 374 (1) (2004) 342–350.
- [26] R. Choube, DHC Axial Velocity Test Procedure for IAEA Round Robin Test Program, FC-IAEA-02 T1.20.13-CAN-273.63-02 (1998).
- [27] A.M.A.H.V. Grigoriev, G. Lysell, D. Schrire, L. Hallstadius, S.T. Mahmood, I. Arimescu, Experimental Study of DHC of Unirradiated and Irradiated Fuel Cladding and Implications to In-Pile Operation and Dry Storage Conditions, *Zirconium in Nuclear Industry*, ASTM STP, 2013 1543.
- [28] C. Coleman, Effect of Texture on Hydride Reorientation and Delayed Hydrogen Cracking in Cold-Worked Zr-2.5 Nb, *Zirconium in the Nuclear Industry*, ASTM International, 1982.
- [29] C. Coleman, B. Cheadle, A. Causey, G. Doubt, R. Fong, S. Venkatapathi, Improving the Service Life and Performance of CANDU Fuel Channels, *Atomic Energy of Canada Ltd.*, 1996.
- [30] S. Sunil, A.K. Bind, H. Khandelwal, R.N. Singh, J.K. Chakravarthy, Delayed hydride cracking behavior of Zr-2.5 Nb alloy pressure tubes for PHWR700, *J. Nucl. Mater.* 466 (2015) 208–219.
- [31] R. Kapoor, A. Sarkar, A.N. Behera, S. Sunil, Multi-axial forging of Nb-1wt.% Zr: effect of annealing on microstructure and mechanical properties, *Mater. Sci. Eng. A* 772 (2020) 138805.
- [32] R.N. Singh, R. Kishore, S. Mukherjee, S. Roychowdhury, D. Srivastava, T.K. Sinha, P. De, S. Banerjee, B. Gopalan, R. Kameswaran, Hydrogen Charging, Hydrogen Content Analysis and Metallographic Examination of Hydride in Zirconium Alloys, *Bhabha Atomic Research Centre*, 2003.
- [33] A.K.B. A. gopalan, R.N Singh, Effect of Hydride Continuity Coefficient(HCC) on Fracture Toughness Behaviour of Zr-2.5 Nb Pressure Tube Material., Un published work (2020).
- [34] S.Q. Shi, M.P. Puls, Criteria for fracture initiation at hydrides in zirconium alloys I. Sharp crack tip, *J. Nucl. Mater.* 208 (3) (1994) 232–242.
- [35] R.N. Singh, H. Khandelwal, A.K. Bind, S. Sunil, P. Stähle, Influence of stress field of expanding and contracting plate shaped precipitate on hydride embrittlement of Zr-alloys, *Mater. Sci. Eng. A* 579 (2013) 157–163.
- [36] S.-Q. Shi, M. Puls, Fracture strength of hydride precipitates in Zr-2.5 Nb alloys, *J. Nucl. Mater.* 275 (3) (1999) 312–317.
- [37] ASTM Standard E-1820, Standard Test Method for Measurement of Fracture Toughness, *ASTM International*, West Conshohocken PA, 2015.
- [38] Z.L. Pan, I.G. Ritchie, M.P. Puls, The terminal solid solubility of hydrogen and deuterium in Zr-2.5 Nb alloys, *J. Nucl. Mater.* 228 (2) (1996) 227–237.
- [39] D. Cameron, R. Duncan, On the existence of a memory effect in hydride precipitation in cold-worked Zr-2.5% Nb, *J. Nucl. Mater.* 68 (3) (1977) 340–344.
- [40] M. Leger, A. Donner, The effect of stress on orientation of hydrides in zirconium alloy pressure tube materials, *Can. Metall. Q.* 24 (3) (1985) 235–243.
- [41] S. Sagat, C.E. Coleman, M. Griffiths, B.J.S. Wilkins, The Effect of Fluence and Irradiation Temperature on Delayed Hydride Cracking in Zr-2.5Nb, *Tenth International Symposium*, ASTM STP 1245 (1994) pp. 35–61.
- [42] D. Yan, R.L. Eadie, The near threshold behaviour of delayed hydride cracking in Zr-2.5 wt% Nb, *Int. J. Press. Vessel.* 77 (4) (2000) 167–177.
- [43] D. Yan, R.L. Eadie, The critical length of the hydride cluster in delayed hydride cracking of Zr-2.5 wt% Nb, *J. Mater. Sci.* 35 (22) (2000) 5667–5672.
- [44] G.K. Shek, M.T. Jovanović, H. Seahra, Y. Ma, D. Li, R.L. Eadie, Hydride morphology and striation formation during delayed hydride cracking in Zr-2.5% Nb, *J. Nucl. Mater.* 231 (3) (1996) 221–230.
- [45] R.N. Singh, P. Stähle, J.K. Chakravarthy, A.A. Shmakov, Threshold stress intensity factor for delayed hydride cracking in Zr-2.5% Nb pressure tube alloy, *Mater. Sci. Eng. A* 523 (1) (2009) 112–117.
- [46] R.N. Singh, R. Lala Mikin, G.K. Dey, D.N. Sah, I.S. Batra, P. Stähle, Influence of temperature on threshold stress for reorientation of hydrides and residual stress variation across thickness of Zr-2.5% Nb alloy pressure tube, *J. Nucl. Mater.* 359 (3) (2006) 208–219.
- [47] M.P. Puls, Effects of crack tip stress states and hydride-matrix interaction stresses on delayed hydride cracking, *Metall. Trans. A* 21 (11) (1990) 2905–2917.
- [48] R. Dutton, K. Nuttall, M.P. Puls, L.A. Simpson, Mechanisms of hydrogen induced delayed cracking in hydride forming materials, *Metall. Trans. A* 8 (10) (1977) 1553–1562.